Available online at www.sciencedirect.com
SCIENCE DIRECT
Polymer 47 (2006) 3548–3556
polymer
www.elsevier.com/locate/polymer

Unique orientation textures formed in miscible blends of poly(vinylidene fluoride) and poly[(*R*)-3-hydroxybutyrate]

Akira Kaito *

Nanotechnology Research Institute, National Institute of Advanced Industrial Science and Technology (AIST), AIST Tsukuba Central 5, 1-1-1 Higashi, Tsukuba, Ibaraki 305-8565, Japan

Received 7 October 2005; received in revised form 10 March 2006; accepted 18 March 2006

Abstract

The oriented crystallization of poly[(*R*)-3-hydroxybutyrate] (PHB) in the miscible blends with poly(vinylidene fluoride) (PVDF) was investigated with various compositions. The PVDF/PHB blend films were prepared by solution casting and subsequent melt-quenching in ice water. Oriented films of the blends were prepared by uniaxially stretching the melt-quenched film at 0 °C in ice water using a hand-operated stretching apparatus. The oriented blend films were heat-treated at a fixed length in order to crystallize PHB in the oriented state. The crystal orientation and the lamellar textures of the obtained samples were studied with wide-angle X-ray diffraction (WAXD), and small-angle X-ray scattering (SAXS), respectively. The SAXS measurements showed that a considerable amount of molecular chains of PHB are excluded from the lamellar stacks of PVDF and exist in the interfibrillar regions in the oriented films of the blends. The cold crystallization of PHB in the interfibrillar region results in the orientation of PHB crystals, and the type of crystal orientation depends upon the composition of the blends. For the PVDF/PHB = 4/6–7/3 blends, the crystal *a*-axis of PHB is highly oriented parallel to the drawing direction and the crystal *c*-axis (molecular chain axis) in PHB crystals is perpendicular to the drawing direction, i.e. orthogonal to the chain axis of the crystals of PVDF. It is considered that the *a*-axis orientation is induced by the confinement of crystal growth in the interfibrillar nano-domains. For the PVDF/PHB = 2/8–3/7 blends, however, the crystal *c*-axis of PHB is primarily oriented in the drawing direction, suggesting that the stressed molecular chains of PHB are crystallized with the molecular orientation retained.

Keywords: Polymer blend; Orientation; Confined crystallization

1. Introduction

Polymer blends have attracted the attention of a lot of scientists because of wide application in various fields. The structure control of polymer blends is essential for improving their macroscopic properties. The orientation of polymer chains is one of the important factors in regulating the physical properties of polymer blends. The orientation control of the polymer chains in the polymer blends has been extensively studied in past decades because of the possibility to produce unique orientation textures that cannot be formed in single-component polymeric materials. The oriented crystallization of polymer blends has been examined for some miscible crystalline/amorphous polymer blends [1–4]. Prud'homme et al. have studied the crystallization and orientation behavior of poly(ε-caprolactone) (PCL) in the miscible blends with poly(vinyl chloride) (PVC) [1,2] and reported that crystallization under strain leads to a crystalline orientation perpendicular to the strain direction under most conditions, whereas a parallel crystalline orientation is observed under conditions where crystallization is rapid and the draw ratio is high. We have examined the oriented crystallization of an isotactic polystyrene (*i*PS)/poly(phenylene oxide) (PPO) blend and produced a unique orientation texture containing highly oriented *i*PS crystals and nearly isotropic PPO chains [3]. More recently, Park et al. studied the oriented crystallization of poly[(*R*)-3-hydroxybutyrated] (PHB) in the blend with cellulose propionate (CP) under strain. It was shown that the manner of oriented crystallization of the PHB component varied from the *c*-axis oriented growth to the *a*-axis oriented crystal growth with increasing the CP content [4]. A number of studies have been reported on the oriented crystallization of immiscible polymer blends consisting of two crystalline polymers, such as polypropylene (PP)/polyethylene (PE) [5–7], PP/isotactic poly(butene-1) [8], PP/nylon 11 [9], polyethylene glycol

* Tel.: +81 298 861 4443; fax: +81 298 861 4437.
E-mail address: a-kaito@aist.go.jp.

0032-3861/$ - see front matter © 2006 Elsevier Ltd. All rights reserved.
doi:10.1016/j.polymer.2006.03.066

(PEG)/nylon [10], PCL/PE [11], and poly(vinylidene fluoride) (PVDF)/nylon 11 [12,13]. If a component with lower melting temperature is crystallized in the oriented matrix of the other component with higher melting temperature, some unusual orientation textures are induced in the dispersed phase.

On the other hand, the structural control of crystalline/crystalline polymer blends possibly produces new types of lamellar morphologies. However, only a limited number of systems is known to us for miscible crystalline/crystalline polymer blends. Manley et al. have recently reported the miscibility, phase behavior, crystallization kinetics, and lamellar morphologies of a miscible crystalline/crystalline blend, PVDF/poly(1,4-butylene adipate) (PBA) [14–18]. Nishi et al. have studied the miscibility, crystallization kinetics, and spherulitic morphology of various crystalline/crystalline polymer blends such as poly(1,4-butylene succinate) (PBSU)/PVDF [19], poly(vinylidene chloride-*co*-vinyl chloride) (PVDCVC)/PBSU [20,21], and poly(ethylene succinate) (PES)/poly(ethylene oxide) (PEO) [22]. They demonstrated the presence of interpenetrated spherulites for PBSU/PVDCVC and PES/PEO blends by optical microscopy and atomic force microscopy observations. PVDF/PHB blends are also known as miscible blend pairs in the molten state, but are crystallized independently into their own crystal lattice. Liu et al. studied the crystallization behavior and spherulitic morphology of PVDF/PHB blends and discussed the lamellar morphologies in relation to their spherulitic morphologies [23,24]. Chiu et al. discussed the morphology of the lamellar stacks of PVDF/PHB blends on the basis of the results of small-angle X-ray scattering (SAXS) [25].

We have recently studied the oriented crystallization of the PBSU/PVDF blend, a miscible crystalline/crystalline polymer blend [26]. The crystallization of PBSU in the confined domains of an oriented blend with PVDF produced a new type of lamellar morphology, in which the two components are segregated in nano-sized domains and are oriented mutually opposite directions. In this work, the oriented crystallization was applied to forming an orthogonal orientation texture in a miscible crystalline/crystalline blend, PVDF/PHB. The oriented films of the blend are obtained by drawing the melt-quenched film in which the molecular chains of PHB keep their amorphous structure. The molecular chains of PHB are isothermally crystallized in the oriented blend films under constraint above room temperature. The crystal orientation and the lamellar morphologies are characterized by wide-angle X-ray diffraction (WAXD) and small-angle X-ray scattering (SAXS), respectively.

2. Experimental section

2.1. Materials and sample preparation

The powder of PVDF with $M_w = 530{,}000$ and that of PHB with $M_w = \sim 500{,}000$ were obtained from Scientific Polymer Products, Inc. (Ontario, USA), and Aldrich Chemical Company, Inc. (St. Louis, USA), respectively. The PVDF/PHB blends with various weight ratios were prepared by casting an *N*,*N*′-dimethylformamide solution with a concentration of 2%. The cast films were dried at 90 °C under vacuum for two days to remove the solvent. The blends were then hot pressed at 185 °C to a film with a thickness of 200 μm, followed by rapid quenching in ice water. PVDF was crystallized during the melt-quenching process, whereas the molecular chains of PHB retained their amorphous structure in the melt-quenched film. The oriented films were prepared by uniaxially stretching the melt-quenched films to the highest elongation, λ_{max}, at 0 °C in ice water using a hand-operated stretching apparatus. The values of λ_{max} increased from 4.8 to 6.4 with increasing the PHB content from 30 to 80 wt%. The melt-quenched films were treated in the ice water bath as much as possible during the drawing experiment in order to prevent the crystallization of PHB. It was confirmed by the measurements of WAXD that the molecular chains of PHB were not crystallized in the drawn films immediately after the drawing experiments. In the next step, the drawn samples were heat-treated with a fixed length for 2 h at temperatures 10 °C below the cold-crystallization peak in differential scanning calorimetry (DSC) heating curves (Fig. 1) in order to crystallize PHB isothermally. The isothermal time-scan of DSC shows that the crystallization was completed in 15–30 min at temperatures 10 °C below the cold-crystallization peak. The isothermal process at each crystallization temperature was set for longer than the time required for the crystallization of PHB in order to ensure that all the crystals were formed during the isothermal process at the designated temperature.

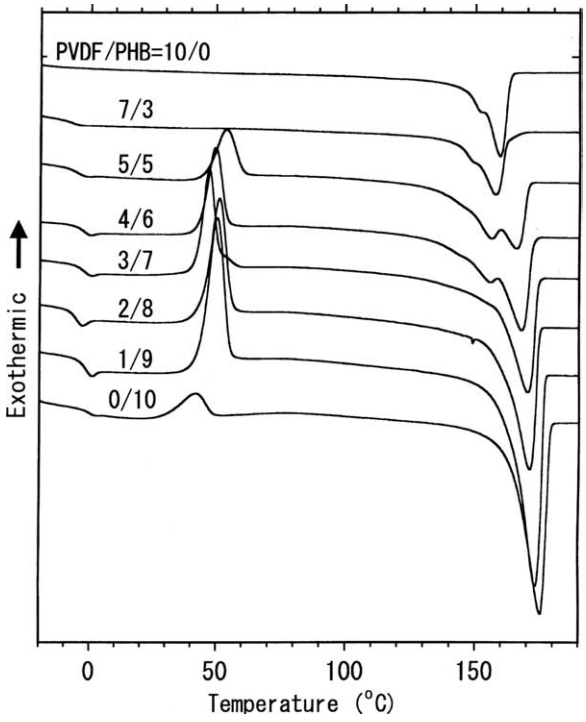

Fig. 1. DSC curves of melt-quenched samples of PVDF, PHB, and PVDF/PHB blends during the heating process at 10 K/min.

2.2. Characterization

Differential scanning calorimetry was measured with a Perkin–Elmer (MA, USA) DSC-7 differential scanning calorimeter calibrated with the melting temperatures of indium and zinc. DSC measurements were carried out under nitrogen flow at heating and cooling rates of 10 K/min.

The WAXD measurements were conducted using Cu Kα radiation (40 kV, 150 mA) with a wavelength of 0.1542 nm generated by an X-ray diffractometer, Rigaku (Akishima, Japan), Ultrax 18SF. The WAXD images were measured with an imaging plate, Rigaku RAXIS-DS3C and the equatorial profiles were obtained directly from the imaging plate. On the other hand, meridional WAXD profiles were measured with a goniometer and a scintillation counter, because meridional reflections are not exposed on the imaging plate for highly oriented samples. The azimuthal intensity distribution for a crystal reflection was also measured with a goniometer and a scintillation counter by rotating the samples at a fixed angle of 2θ.

SAXS were measured with fine-focused Cu Kα radiation (45 kV, 60 mA) generated by an X-ray diffractometer, Rigaku, Ultrax 4153A 172B. A scattering angle resolution of $2\theta = 0.09°$ was achieved with a pair of beam-focusing mirrors, Confocal MAX Flux Optics and three collimation slits. The SAXS images were detected with an imaging plate detector, Rigaku RAXIS-DS3C. The SAXS profiles were obtained directly from the imaging plate.

3. Results and discussion

3.1. Thermal properties

Fig. 1 shows the DSC curves of the melt-quenched samples of PVDF, PHB and PVDF/PHB blends during the heating process. The DSC curves were normalized by sample weight. The WAXD measurement shows the crystallinity of PVDF in the melt-quenched films of the blend, whereas PHB keeps its amorphous structure in the melt-quenched films. The exothermic peaks around 40–60 °C show that PHB crystallizes during the heating process for pure PHB and PVDF/PHB blends with a weight ratio of 1/9–5/5, but the crystallization of PHB is restricted for the blends with higher PVDF content. The glass transition temperature (T_g) of PHB is observed around 0 °C and gradually shifts to lower temperatures with increasing PVDF content. The melting temperatures (T_m) of pure PVDF and PHB are 160 and 176 °C, respectively, whereas the melting peaks in the blend decrease with respect to the melting peaks of the pure polymers owing to the miscibility of the blends. Chien et al. [25] and Liu and Jungnickel [23,24] reported the miscibility and crystallization behavior of the PVDF/PHB blends. The results of this work also support the miscibility of the blend system.

Fig. 2 shows the DSC curves of PVDF, PHB and PVDF/PHB blends during the cooling process from the molten state. The results of the DSC curves indicate that both PHB and PVDF crystallize during the melt-crystallization process for the PVDF/PHB = 2/8–5/5 blends but the crystallization of the minor component is restricted outside the composition ranges. PVDF is crystallized in the first step, and PHB crystallizes in the pre-existing morphology of PVDF. The crystallization temperatures (T_c) of PVDF and PHB decrease in the blends with increasing the content of the counter component, owing to the dilution effects.

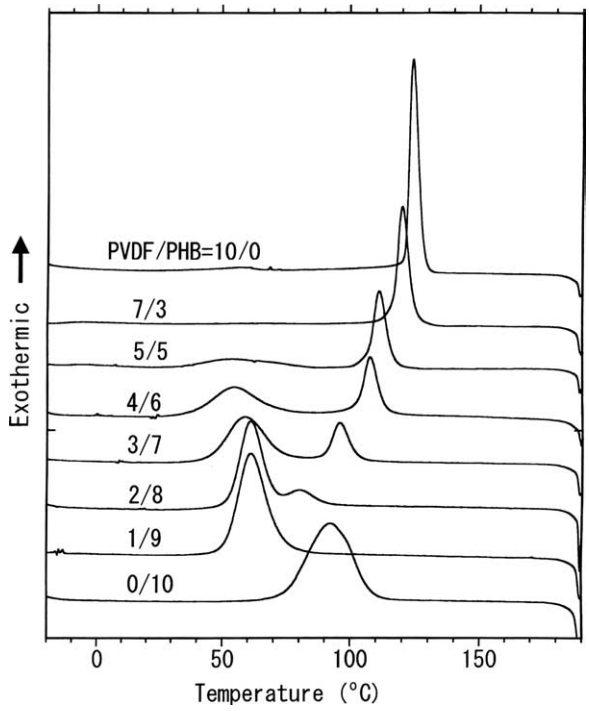

Fig. 2. DSC curves of PVDF, PHB, and PVDF/PHB blends during the cooling process from the molten state at 10 K/min.

3.2. Crystal orientation

Fig. 3 shows the WAXD patterns of the PVDF/PHB blends crystallized under the highest elongation. The samples are drawn in ice water to the highest draw ratio and PHB was crystallized in the oriented films at the highest draw ratio with a fixed length at temperatures 10 °C below the crystallization peaks of the DSC curves. The equatorial profiles obtained directly from the WAXD images are shown in Fig. 4 with the assignments of the observed reflections. The WAXD reflections of the α and β crystalline forms of PVDF are observed in Figs. 3 and 4, indicating that the two crystalline forms of PVDF coexist in the oriented samples of PVDF and PVDF/PHB blends. The α crystalline form exhibits 100, 020, and 110 reflections at $2\theta = 17.9$, 18.4, and 20.1°, respectively, on the equator, whereas the β crystalline form shows 110 and 200 reflections at $2\theta = 20.8°$ on the equator. The *hk*0 reflections of the α and β crystalline forms of PVDF are observed on the equator, indicating that the crystal *c*-axis (molecular chain axis) of the two crystalline forms of PVDF are oriented in the drawing direction for all blend samples. On the other hand, the molecular chains of the melt-crystallized PHB are packed in an orthorhombic crystal lattice with the parameters $a = 0.576$ nm,

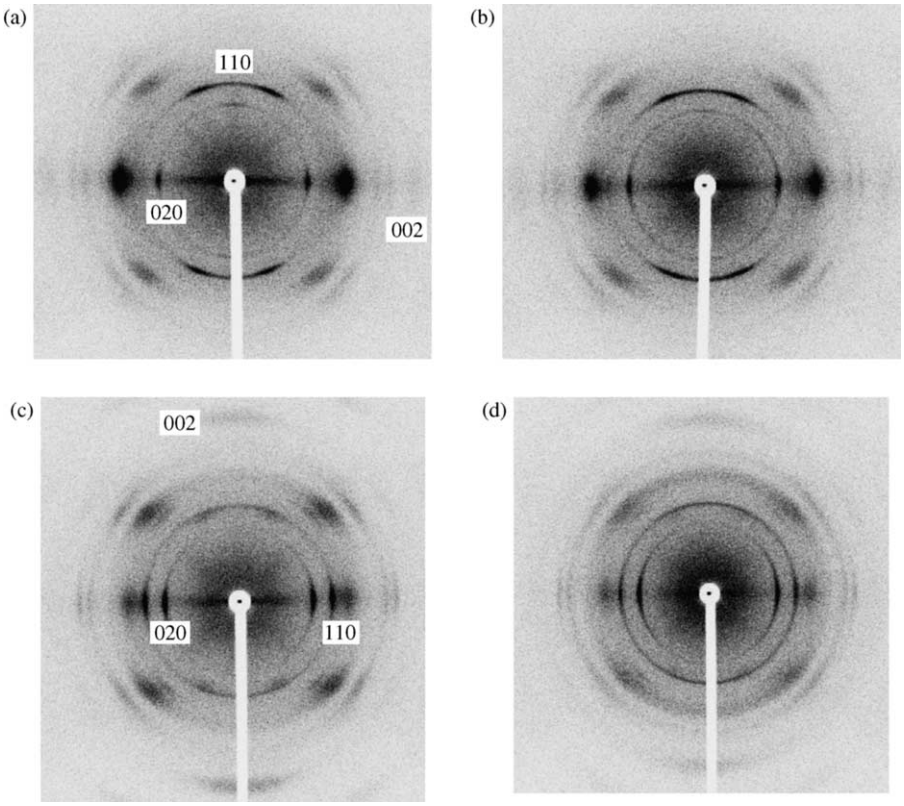

Fig. 3. WAXD images of PVDF/PHB blends crystallized at the highest elongation, λ_{max}: (a) PVDF/PHB = 5/5 λ_{max} = 4.9, (b) PVDF/PHB = 4/6 λ_{max} = 5.1, (c) PVDF/PHB = 3/7 λ_{max} = 5.7, (d) PVDF/PHB = 2/8 λ_{max} = 6.4. The reflections of PHB are indexed in (a) and (c).

b = 1.320 nm, and c = 0.596 nm [27]. The 020, 110, and 002 reflections of PHB are clearly observed at 2θ = 13.5, 17.0, and 30.3°, respectively, in the WAXD image (Fig. 3) and the equatorial profiles (Fig. 4). The WAXD images indicate that the types of crystal orientation of PHB changes with blend composition. For the PVDF/PHB = 4/6–7/3 blends, the spots of the 110 reflection (2θ = 13.5°) are located at 20–30° from the meridian along the azimuthal angle and the 020 reflection exhibits intense spots on the equator (Fig. 3). Furthermore, the 002 reflection is observed in the equatorial WAXD profiles of the samples (Fig. 4). These results suggested that the crystal a-axis of PHB is oriented in the drawing direction and that the crystal c-axis (molecular chain axis) is perpendicular to the drawing direction for the PVDF/PHB = 4/6–7/3 blends. The 020 reflections are observed also on the meridian for PVDF/PHB = 5/5–7/3, suggesting that a small amount of the b-axis orientation coexists with the a-axis orientation for the samples. The PVDF/PHB = 2/8–3/7 blends, however, exhibits a strong 110 reflection on the equator and its intensity in the meridional range markedly decreases (Fig. 3). The crystal c-axis of the samples with PVDF/PHB = 2/8–3/7 is mainly oriented in the drawing direction, because the 110 and 020 reflections lie on the equator.

Fig. 5 shows the meridional WAXD profiles of the PVDF/PHB blends measured with a goniometer scan. The 001 reflection of the β crystalline form of PVDF and the 002 reflection of the α form are observed at 35.0 and 38.9°, respectively. Only the reflection of the β crystalline form is observed for the highly oriented pure PVDF, whereas the two crystalline forms coexist in the PVDF/PHB blends. The relative intensity of these reflections suggests that the crystallinity of the α crystalline form decreases and that of the β

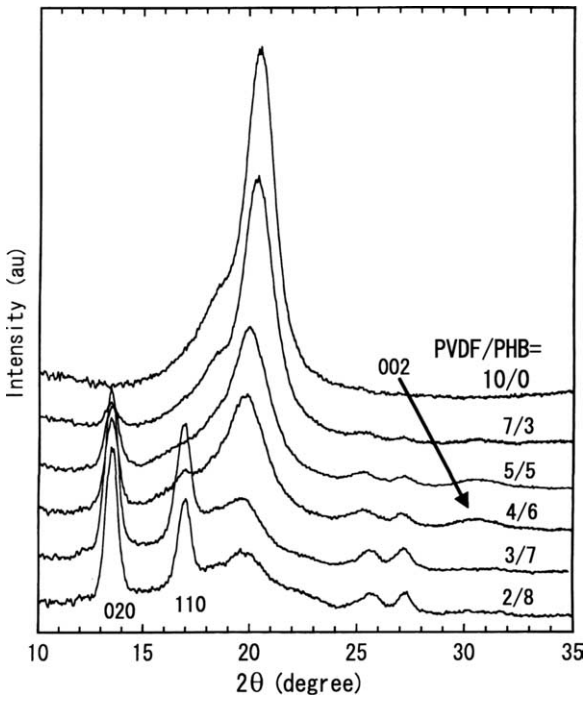

Fig. 4. Equatorial WAXD profiles of PVDF and PVDF/PHB blends crystallized at highest elongation.

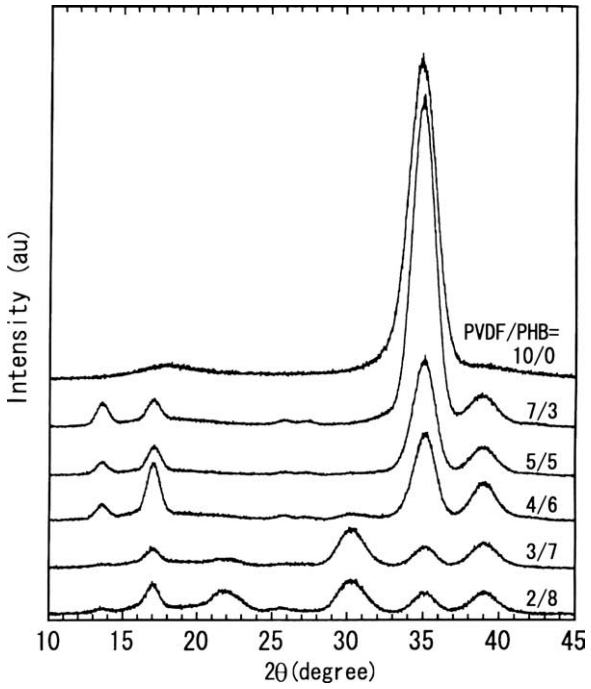

Fig. 5. Meridional WAXD profiles of PVDF and PVDF/PHB blends crystallized at the highest elongation.

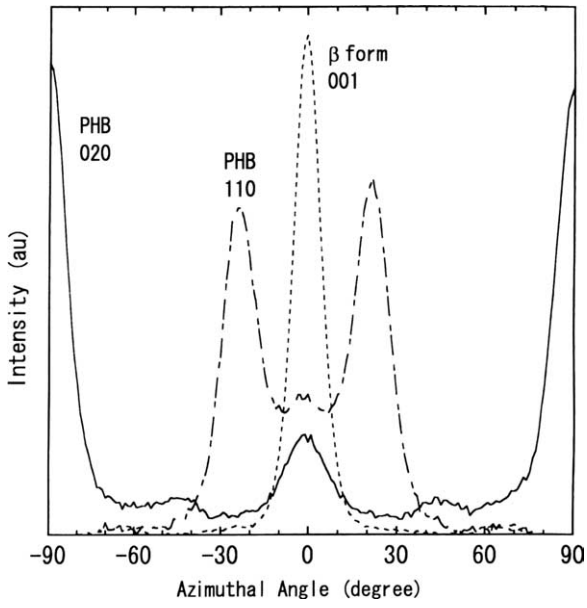

Fig. 6. Azimuthal angle profiles of WAXD reflections for the PVDF/PHB = 5/5 blend crystallized at highest elongation, $\lambda_{max} = 4.9$: (—) 020 reflection of PHB; (– - –) 110 reflection of PHB; (- - -) 001 reflection of the β crystalline form of PVDF.

crystalline form increases with increasing PVDF content. The appearance of the 002 reflection of PHB confirms that the crystal *c*-axis of PHB is oriented in the drawing direction for the PVDF/PHB = 2/8–3/7 blends.

The intensity profiles of the WAXD reflections along the azimuthal angle were obtained after the background corrections. The intensity distribution, $I(\theta,\varphi)$ is expressed as a function of the Bragg angle, θ, and the azimuthal angle, φ. The subtraction of the background intensity was carried out as follows

$$I(\varphi)_c = I(\theta_p,\varphi) - I(\theta_{b1},\varphi)C_1 - I(\theta_{b2},\varphi)C_2 \quad (1)$$

$$C_1 = \frac{\theta_{b2}}{\theta_{b1}+\theta_{b2}} \quad (2)$$

$$C_2 = \frac{\theta_{b1}}{\theta_{b1}+\theta_{b2}} \quad (3)$$

$I(\theta_p,\varphi)$ is the azimuthal intensity distribution of the crystalline reflection of interest, whose peak is observed at θ_p, and $I(\theta_{b1},\varphi)$ and $I(\theta_{b2},\varphi)$ are the intensity distributions of backgrounds at θ_{b1} and θ_{b2} ($\theta_{b1} < \theta_p < \theta_{b2}$).

Fig. 6 shows azimuthal intensity profiles of the 020 and 110 reflections of PHB for the PVDF/PHB = 5/5 blend. The 020 reflection of PHB shows peaks at $\pm 90°$ (transverse direction), indicating that the crystal *b*-axis is oriented perpendicular to the drawing direction. The peaks at $\pm 23°$ (near meridian) for the 110 reflection of PHB suggest that the crystal *a*-axis of PHB is oriented in the drawing direction, because the reciprocal lattice vector of the 110 reflection of PHB is tilted 23.6° away from the crystal *a*-axis. The Hermans–Stein orientation function, *f*, for the crystal axes of PHB is calculated from the corrected intensity distribution

$$\langle\cos^2\varphi\rangle = \frac{\int_0^{\pi} I(\varphi)_c \cos^2\varphi \sin\varphi \mathrm{d}\varphi}{\int_0^{\pi} I(\varphi)_c \sin\varphi \mathrm{d}\varphi} \quad (4)$$

$$f = \frac{3\langle\cos^2\varphi\rangle - 1}{2} \quad (5)$$

the orientation function of the crystal *b*-axis, f_b, can be calculated from the azimuthal intensity distribution of the 020 reflection. The orientation function of the crystal *c*-axis, f_c, was calculated from the azimuthal intensity profiles of the 110 and 020 reflections by use of the Wilchinsky equation [28]. The value of f_a was obtained from the relationship of the orientation functions of the crystal axes for the orthorhomibic crystal lattice

$$f_a + f_b + f_c = 0.0 \quad (6)$$

The calculated values of f_a, f_b, and f_c are 0.76, −0.32, and −0.44, respectively, and indicate the high degree of orientation of the crystal *a*-axis parallel to the drawing direction for the PVDF/PHB = 5/5 blend. The azimuthal intensity profile for the 001 reflection of the β crystalline form of PVDF is also plotted in Fig. 6, which shows that the crystal *c*-axis of the β crystalline form is highly oriented in the drawing direction.

Fig. 7 shows azimuthal intensity profiles of WAXD reflections for the PVDF/PHB = 3/7 blend. The 020 reflection shows intense peaks at $\pm 90°$, similar to the PVDF/PHB = 5/5 blend. However, the intensity profile of the 110 reflection for the PVDF/PHB = 3/7 blend is much different from that for the PVDF/PHB = 5/5 blend. The 110 reflection for the

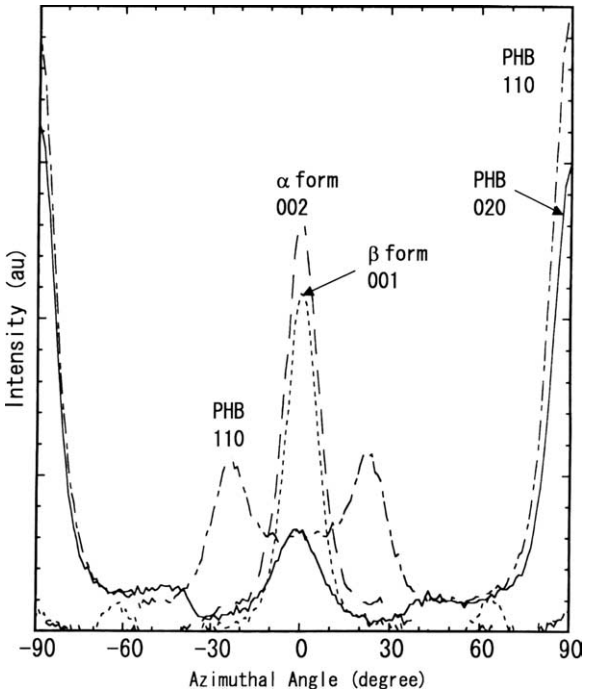

Fig. 7. Azimuthal angle profiles of WAXD reflections for the PVDF/PHB = 3/7 blend crystallized at the highest elongation, $\lambda_{max} = 5.7$: (—) 020 reflection of PHB; (– – –) 110 reflection of PHB; (- - -) 001 reflection of the β crystalline form of PVDF; (– – –) 002 reflection of the α crystalline form of PVDF.

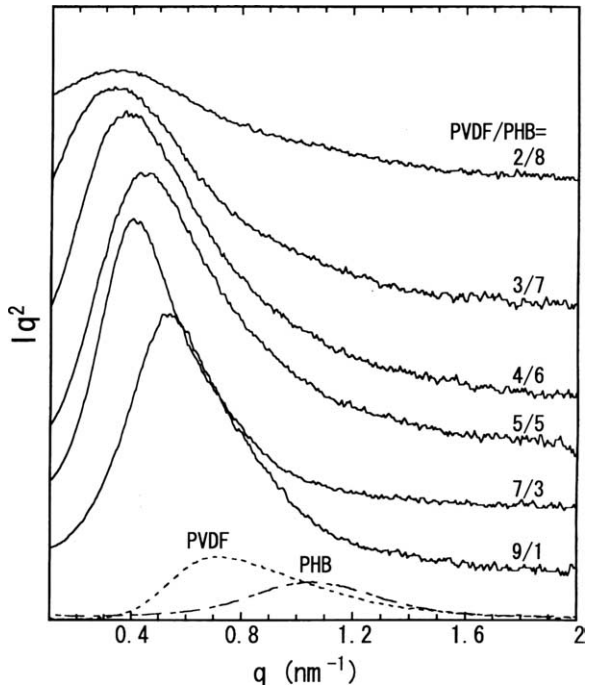

Fig. 8. SAXS profiles of isotropic samples prepared by melt-quenching and cold-crystallization: (- - -) PVDF; (– – –) PHB; (—) PVDF/PHB blends.

PVDF/PHB = 3/7 blend exhibits intense peaks at ±90° (transverse direction), and weak meridional peaks at ±23°. Although the *a*-axis orientation coexists with the *c*-axis orientation, the fraction of the *c*-axis orientation is higher than that of the *a*-axis orientation for the PVDF/PHB = 3/7 blend. The orientation functions, f_a, f_b, and f_c, for the PVDF/PHB = 3/7 blend are −0.18, −0.33, and 0.51, respectively, and confirm that the major mode of the crystal orientation is the *c*-axis orientation in the drawing direction. Fig. 7 includes the azimuthal intensity profiles for the 002 and 001 reflections of the α and β crystalline forms, respectively, of PVDF. It is difficult to determine the orientation function, f_c, for the PVDF crystals because of the overlaps of these reflections with neighboring reflections. The azimuthal intensity profiles, however, indicate that the crystal *c*-axis of the α and β crystalline forms of PVDF is highly oriented in the drawing direction.

3.3. SAXS results

Fig. 8 shows the Lorentz-corrected SAXS profiles of isotropic samples of the PVDF/PHB blends prepared by melt-quenching and cold-crystallization. The SAXS intensity was normalized by the sample thickness and exposure time, after subtracting air scattering. PVDF and PHB exhibit a SAXS peak at $q = 0.7$ and 0.95 nm^{-1}, respectively, which correspond to long periods, $L = 9.0$ and 6.6 nm, respectively. On the other hand, the PVDF/PHB blends show an intense peak at $q = 0.3$–0.55 nm^{-1} ($L = 11$–21 nm) and the peak position shifts to the lower *q* range (i.e. longer *L*) with increasing the PHB content. The scattering intensity of the blends is much higher than those of PVDF and PHB, indicating that the magnitude of electron density fluctuation significantly increases for the blend relative to the pure polymers. The long period for the PVDF/PHB = 5/5 blend is approximately the sum of the long periods of the pure polymers. It was considered that the amorphous molecular chains of PHB are incorporated between the lamellae of PVDF during melt-quenching and further crystallized in the thick interlamellar regions of PVDF crystals during heat-treatment. Thus, the crystallization of PHB in the isotropic films of PVDF/PHB blends forms a lamellae inclusion structure in which the lamellae of PVDF and PHB are alternately stacked. Chiu et al. reported that melt-crystallization of PVDF/PHB blends generated two kinds of lamellar stacks with one containing primarily PVDF lamellae and the other consisting of PHB lamellae [25]. However, only the lamellar inclusion structure exists for the present samples, because the amorphous chains of PHB were mainly incorporated between the lamellae of PVDF during the melt-quenching process. The lamellar inclusion structure has also been reported for other miscible crystalline/crystalline polymer blends, such as PVDF/PBA [17,18], PVDF/PBSU [26], and PEO/PBSU [29].

Fig. 9 shows the SAXS images of the PVDF/PHB blends crystallized at the highest elongation. A very strong scattering can be observed in the equatorial direction in addition to the meridional scattering. The scattering in the equatorial direction indicates that large electron density fluctuation is induced perpendicular to the stretching direction and that periodic structures are formed perpendicular to the stretching direction. Fig. 10 shows the meridional SAXS profiles obtained directly from the SAXS images. The drawn film of pure PVDF shows a SAXS peak at $q = 0.90$ nm^{-1} ($L = 7.0$ nm), whereas the

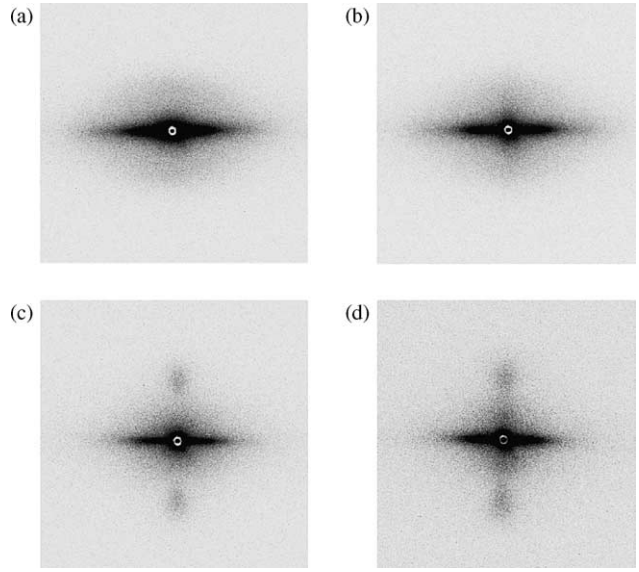

Fig. 9. SAXS images of PVDF/PHB blends crystallized at the highest elongation, λ_{max}. (a) PVDF/PHB = 5/5 λ_{max} = 4.9; (b) PVDF/PHB = 4/6 λ_{max} = 5.1; (c) PVDF/PHB = 3/7 λ_{max} = 5.7; (d) PVDF/PHB = 2/8 λ_{max} = 6.4.

corresponding SAXS peak shifts to $q = 0.65$–$0.75\ nm^{-1}$ (L = 8.4–9.7 nm) for the oriented films of the PVDF/PHB = 4/6–7/3 blends. The long periods of the oriented PVDF/PHB blends are longer than that for the oriented PVDF, but are shorter than those for the isotropic PVDF/PHB blends with same composition (Fig. 8). It is considered that the SAXS peak originates from the lamellar stacks of PVDF crystals containing the molecular chains of PHB in the amorphous layer. On the other hand, intense SAXS peaks are observed at $q = 1.0\ nm^{-1}$ (L = 6.3 nm) for the oriented samples of PVDF/PHB = 2/8 and 3/7 blends. The SAXS peak is attributed to the lamellar stacks of PHB crystals with *c*-axis orientation, because the peak position is close to that of pure PHB.

As shown above, the lamellar morphology of the oriented crystallized samples of PVDF/PHB blends is different from that of isotropic blends. Fig. 11 shows a schematic illustration for the morphology changes during stretching. Amorphous chains of PHB are included in the interlamellar regions of the thick lamellae of PVDF for the isotropic films. However, the molecular chains of PHB are considerably excluded from the lamellar stacks of PVDF and exist in the interfibrillar regions in the oriented films of the blends. The interfibrillar exclusion morphology might be stabilized for the oriented samples, because tie-molecules should be produced between crystallites and act as stress transmitters during drawing. The segregation of the lamellar stacks during stretching was reported for PVDF/PBSU blends [26]. The long period is markedly decreased by drawing the films of PVDF/PHB blends, but is still longer than the long period of pure PVDF because of the presence of a small amount of molecular chains of PHB in the interlamellar region of PVDF.

Fig. 12 shows the equatorial SAXS profiles obtained directly from the SAXS images. The oriented samples of PVDF/PHB blend exhibit the intense equatorial scattering, whereas, the drawn film of PVDF does not show any significant scattering in this range. The densities of PVDF and PHB are 1.8 and 1.2 g/cm^3, respectively. If we consider the large density difference of PVDF and PHB, it is reasonable to attribute the intense equatorial scattering to the periodic arrangement of the PHB-rich and PVDF-rich fibrillar domains, as shown in Fig. 11. A shoulder is observed at $q = 1.2$–$1.3\ nm^{-1}$ (L = 4.8–5.2 nm)

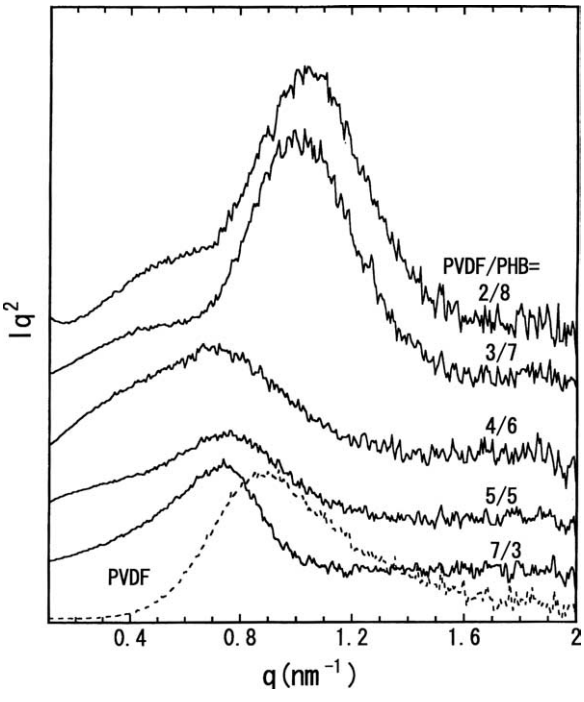

Fig. 10. Meridional SAXS profiles of oriented samples crystallized at the highest elongation: (- - -) PVDF; (—) PVDF/PHB blends.

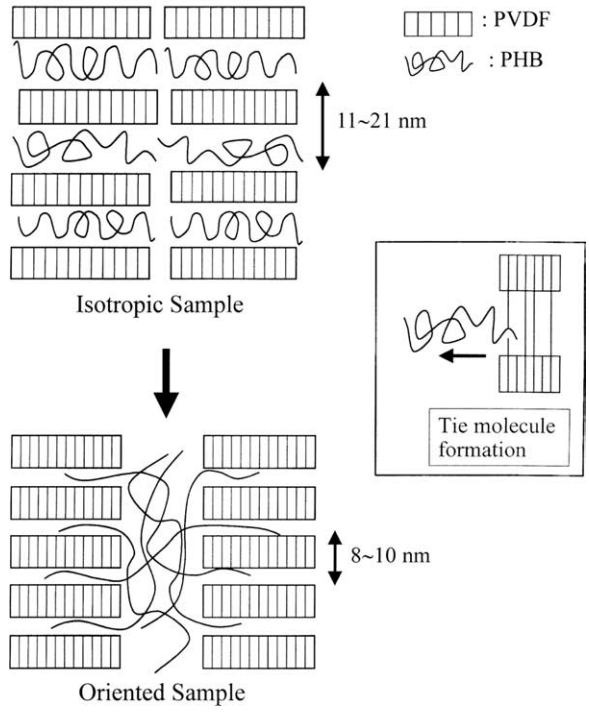

Fig. 11. Schematic illustration for transformation of lamellar morphologies during stretching.

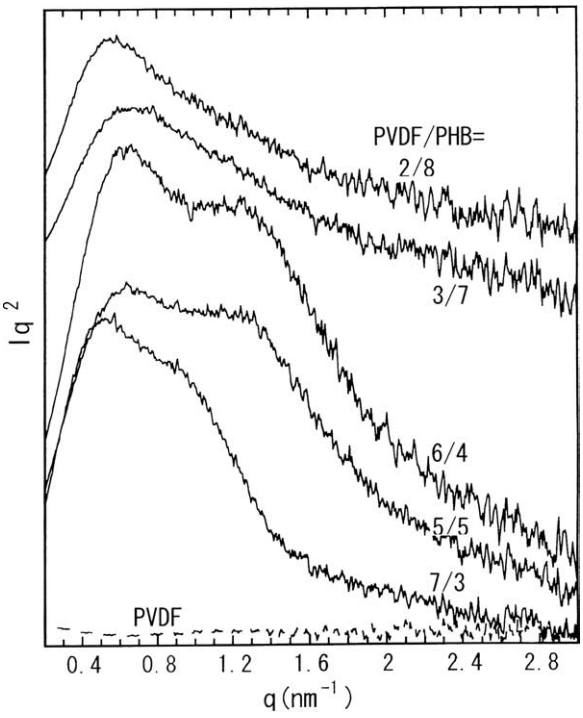

Fig. 12. Equatorial SAXS profiles of oriented samples crystallized at the highest elongation: (- - -) PVDF; (—) PVDF/PHB blends.

for the equatorial profile of PVDF/PHB = 4/6–7/3 blends. The shoulder can be assigned to the stacks of a few lamellae of PHB, because the shoulder is observed only for the samples with perpendicular orientation of PHB crystals. It is considered that the lamellae of PHB are crystallized in the fibrillar domains that are periodically arranged perpendicular to the drawing direction.

3.4. Mechanism for orientated crystallization

It is important to consider the mechanism of the formation of the unique orientation textures. Crystal growth, such as epitaxial crystallization [9–11], trans-crystallization [8,12,13], crystallization under thermal shrinkage stress [5–7], and confined crystallization [4,26,29], has been proposed as a possible mechanism for the formation of the orientation textures. For example, epitaxial crystallization has been considered to form oriented structures in some immiscible crystalline/crystalline polymer blends [9–11]. However, the possibilities of lattice matching are not found for PVDF and PHB crystal lattices. Furthermore, crystal orientation of PHB depends upon the blend composition, suggesting that the other mechanism is working for the PVDF/PHB blend. Therefore, the epitaxial crystallization of PHB on the surface of PVDF crystals can be ruled out. Trans-Crystallization has been often used to interpret the oriented crystallization in crystalline polymer blends [8,12,13]. We have reported that a new type of orientation texture of PVDF crystals has been developed in the oriented blend of PVDF/Nylon 11 due to trans-crystallization [12,13]. However, the size of the domains, in which trans-crystallization occurs, is much larger than the nano-sized domains formed in miscible crystalline polymer blends.

Another mechanism that should be considered is the confinement of crystal growth in the nano-sized domains. It was reported that crystal orientation was induced by the confinement of crystal growth in the narrow channels formed between inorganic fibers [30,31] or the drawn polymer matrix [32]. We have recently studied the oriented crystallization of PBSU in the oriented blend with PVDF at various temperatures. The confinement of the crystal growth of PBSU in the nano-sized interfibrillar domains results in a unique orthogonal orientation texture [26]. More recently, Park et al. studied the oriented crystallization of PHB under uniaxial drawing in miscible blends with cellulose propionate (CP), and developed a unique orientation texture with lamellar stacking perpendicular to the drawing direction [4]. The orientation behavior was interpreted as originating from intramolecular nucleation and confined crystal growth. The confined crystal growth in the nano-sized domain is considered as a possible mechanism for the formation of orthogonal orientation of PVDF/PHB blends, because the molecular chains of PHB are confined in narrow regions.

The mechanism of orientated crystallization is summarized in Fig. 13. The lamellar stacking structures in the figure are illustrated based on the SAXS results (Figs. 10 and 12). The molecular chains of PHB are partially excluded from the lamellar stacks of PVDF and reside in the interfibrillar regions. For PVDF/PHB = 4/6–7/3, the crystalline morphology of PVDF mainly acts as a stress transmitter during heat-treatment and the molecular chains of PHB may be partially relaxed

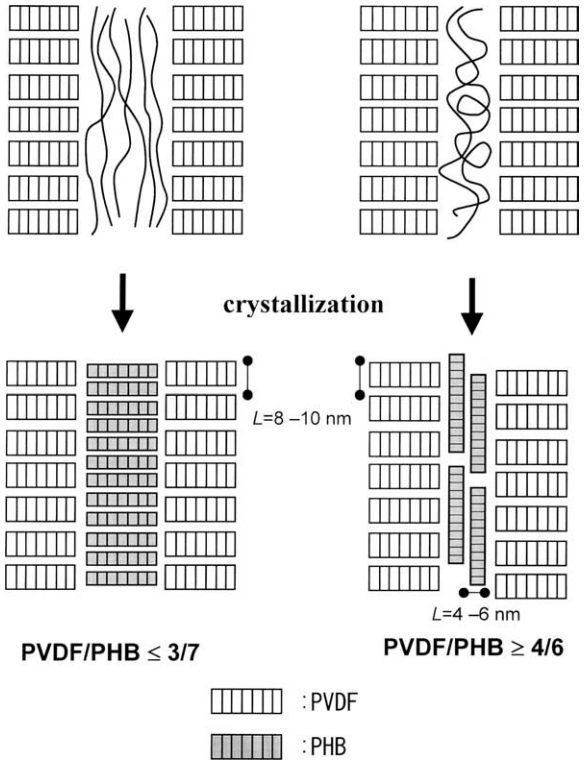

Fig. 13. Schematic illustration for composition effects on oriented crystallization of PHB in PVDF/PHB blends.

during heat-treatment, because a major component is able to form a continuous phase. The crystallization of PHB occurs mainly in interfibrillar regions and crystal growth is considered to proceed along the fibrillar axis, i.e. drawing direction, because of the confinement of crystal growth. Birley et al. suggested that the chain-folded crystals of PHB grow along the crystal *a*-axis [33]. Thus, the confined crystallization of PHB in inerfibrillar regions results in the *a*-axis orientation of PHB crystals along the fiber axis. The mechanism of oriented crystallization for the PVDF/PHB blends is considered to be similar to that for the PHB/CP blends reported by Park et al. [4]. The rigid chains of CP form elongated narrow regions for the confined crystallization of PHB in the case of PHB/CP blend, whereas the oriented lamellar stacks of PVDF constitute the nano-domains in the interfibrillar regions for the PVDF/PHB blends. On the other hand, the molecular chains of PHB become stressed during crystallization under stress with increasing PHB content, as shown in Fig. 13. The stressed molecular chains of PHB will crystallize in the nano-domains with the orientation retained for the PVDF/PHB = 2/8–3/7 blends. Thus, the oriented crystallization of PHB in the oriented films of the PVDF/PHB blends is determined by the balance of the confinement of crystal growth and the orientation of stressed molecular chains during crystallization. The former exceeds the latter for PVDF/PHB blends with lower PHB content, whereas the latter is more effective than the former for oriented crystallization at higher PHB content.

4. Conclusions

Unique orientation structures of lamellar crystals were developed by oriented crystallization of PHB in the oriented films of the PVDF/PHB blends. The SAXS measurements show that a considerable amount of molecular chains of PHB are excluded from the lamellar stacks of PVDF and exist in the interfibrillar regions in the oriented films of the blends. The cold-crystallization of PHB in the interfibrillar region results in the orientation of PHB crystals, and the type of orientation depends upon the composition of the blends. The crystal *a*-axis of PHB is highly oriented in the drawing direction for the PVDF/PHB = 4/6–7/3 blends, whereas the crystal *c*-axis (molecular chain axis) is primarily oriented in the drawing direction for the PVDF/PHB = 2/8–3/7 blends. It is considered that the *a*-axis orientation is induced by the confinement of crystal growth in the interfibrillar nano-domains and that the *a*-axis, the axis of crystal growth, is oriented parallel to the fiber-axis of the nano-sized fibrillar domains. Thus, the lamellar crystals of the two polymers are oriented in mutually opposite directions. On the other hand, the oriented molecular chains of PHB are crystallized with the molecular orientation retained during heat-treatment for the PVDF/PHB = 2/8–3/7 blends.

References

[1] Zhao Y, Keroack D, Prud'homme R. Macromolecules 1999;32(4):1218–25.
[2] Morin D, Zhao Y, Prud'homme R. J Appl Polym Sci 2001;81(7):1683–90.
[3] Dikshit A, Kaito A. Polymer 2003;44(21):6647–56.
[4] Park JW, Doi Y, Iwata T. Macromolecules 2005;38(6):2345–54.
[5] Nishio Y, Yamane T, Takahashi T. J Macromol Sci-Phys 1984;B23(1):17–27.
[6] Kojima M, Satake H. J Polym Sci, Polym Phys 1984;22(2):285–94.
[7] Gross B, Petermanm J. J Mater Sci 1984;19(1):105–12.
[8] Takahashi T, Nishio Y, Mizuno H. J Appl Polym Sci 1987;34(8):2757–68.
[9] Seth KK, Kempster CJE. J Polym Sci, Polym Symp 1977;58:297–310.
[10] Fornes RE, Grady PL, Hersh SP, Bhat GR. J Polym Sci, Polym Phys 1976;14(3):559–63.
[11] Takahashi T, Inamura M, Tsujimoto I. J Polym Sci, Polym Lett 1970;8(9):651–7.
[12] Li YJ, Kaito A. Macromol Rapid Commun 2003;24(3):255–60.
[13] Li YJ, Kaito A. Polymer 2003;44(26):8167–76.
[14] Penning JP, Manley RSJ. Macromolecules 1996;29(1):77–83.
[15] Penning JP, Manley RSJ. Macromolecules 1996;29(1):84–90.
[16] Fujita K, Kyu T, Manley RSJ. Macromolecules 1996;29(1):91–6.
[17] Liu LZ, Chu B, Penning JP, Manley RSJ. Macromolecules 1997;30(15):4398–5504.
[18] Liu LZ, Chu B, Penning JP, Manley RSJ. J Polym Sci, Part B: Polym Phys 2000;38(14):2296–308.
[19] Lee JC, Tazawa H, Ikehara T, Nishi T. Polym J 1998;30(4):327–39.
[20] Lee JC, Tazawa H, Ikehara T, Nishi T. Polym J 1998;30(10):780–9.
[21] Ikehara T, Nishi T. Polym J 2000;32(8):683–7.
[22] Qiu Z, Ikehara T, Nishi T. Macromolecules 2002;35(22):8251–4.
[23] Liu J, Jungnickel BJ. J Polym Sci, Part B: Polym Phys 2003;41(9):873–82.
[24] Liu J, Jungnickel BJ. J Polym Sci, Part B: Polym Phys 2004;42(6):974–85.
[25] Chiu HJ, Chen HL, Lin JS. Polymer 2001;42(13):5749–54.
[26] Li YJ, Kaito A, Horiuchi S. Macromolecules 2004;37:2119.
[27] Yokouchi M, Chatani Y, Tadokoro H, Teranishi K, Tani H. Polymer 1973;14(6):267–72.
[28] Wilchinsky ZW. J Appl Phys 1960;31(11):1969–72.
[29] He Y, Zhu B, Kai W, Inoue Y. Macromolecules 2004;37(9):3337–45.
[30] Lhymn C, Schultz JM. Polym Compos 1985;6:87.
[31] Waddon AJ, Hill MJ, Keller A, Blundell DJ. J Mater Sci 1987;22(5):1773–84.
[32] Mencik Z, Plummer HK, Oene HV. J Polym Sci, Part A-2 1972;10(3):507–17.
[33] Birley C, Briddon J, Sykes KE, Barker PA, Organ SJ, Barham PJ. J Mater Sci 1995;30(3):633–8.